PHYSICAL REVIEW B **83**, 174204 (2011)

Stress-induced strain glass to martensite (R) transition in a $Ti_{50}Ni_{44.5}Fe_{5.5}$ alloy

Jian Zhang,[1,2,4] Yu Wang,[1,2] Xiangdong Ding,[1,2] Zhen Zhang,[1,2] Yumei Zhou,[1,2] Xiaobing Ren,[1,2,*] Kazuhiro Otsuka,[1,2] Jun Sun,[1] and Minghui Song[3]

[1]*Multi-disciplinary Materials Research Center, Frontier Institute of Science and Technology, State Key Laboratory for Mechanical Behavior of Materials, Xi'an Jiaotong University, Xi'an 710049, China*

[2]*Ferroic Physics Group, National Institute for Materials Science, Tsukuba 305-0047, Ibaraki, Japan*

[3]*Advanced Electron Microscopy Group, National Institute for Materials Science, Tsukuba 305-0047, Ibaraki, Japan*

[4]*Institute for Materials, Ruhr-University Bochum, D-44801 Bochum, Germany*

(Received 1 February 2011; revised manuscript received 7 April 2011; published 16 May 2011)

Strain glass (STG) in Ni-rich binary Ti-Ni possesses an R-like (rhombohedral) local strain order, but it transforms into $B19'$ martensite under stress. It remains a puzzle why the local strain order in STG yields a different long-range strain order. Here, we systematically investigated a ternary $Ti_{50}Ni_{44.5}Fe_{5.5}$ STG, which exhibited the same STG features as the binary STG, and the local strain order is also an R-like one. Different from the binary STG, under stress this ternary STG transforms into a *normal* R phase rather than $B19'$. By considering that both systems have bi-instability with respect to both R and $B19'$ martensites in the schematic free-energy landscape, we provide a unified explanation for the different products of the stress-induced STG to martensite (STG-M) transition between a Ti-Ni binary system and the present ternary system. We show that the differences stem from the competing thermodynamic stability between R-phase and $B19'$ martensites.

DOI: 10.1103/PhysRevB.83.174204 PACS number(s): 64.70.P−, 64.60.My, 64.60.Cn

I. INTRODUCTION

Glass is a frozen metastable state exhibiting high frustration, which leads to the inability of the system to reach the ground state, a long-range order.[1] Hence it exhibits the breaking of ergodicity;[2–4] this challenges the basic assumption of statistical mechanics. Glassy phenomena have been discovered in various systems, such as ferroelectric, magnetic, superconductive, and biological systems, etc.,[5–9] and have been well investigated for both fundamental and practical interest.

Recently, a "strain glass" (STG) was discovered in a binary ferroelastic/martensitic system of $Ti_{50}-xNi_{50}+x$ ($x \geqslant 1.5$) alloy, which originates from the random local stresses of point defects.[10–12] These random local stresses dictate the local strain orders and hence prohibit the formation of long-range strain ordering. Thus, spontaneous martensitic transition becomes inaccessible kinetically, although martensite is favored thermodynamically at low temperatures.[13] The STG transition was proved experimentally by frequency dispersion[10] in its ac mechanical properties and breaking down of ergodicity.[3] These key glassy features of STG were recently reproduced theoretically by Landau-Ginsburg simulations.[14,15] Microscopically, the Ti-Ni binary STG transforms (freezes) into a configuration of random nanoclusters with local R (rhombohedral) -like phases, distributed randomly in a parent B2 matrix.[10]

Being physically parallel to cluster spin glass and relaxor, STG also shows some novel properties. Very recently, it was found that binary Ti-Ni STG exhibits a new shape memory effect and superelasticity, which originates from a stress-induced transition from STG (with R-like local order) to a long-range strain-ordered phase, $B19'$ (monoclinic) martensite.[11] It shares the same physical origin as the field-induced transition in relaxor, whereas the order parameter is polarization.[16–18]

For binary Ti-Ni STG, although it is conceivable that a local order can be changed into a long-range order by stress, it remains a puzzle why the R-like local order does not transform into an R phase (with the same strain order), and why it changes into a $B19'$ martensite (with different strain order). To uncover the origin of this abnormal behavior, we seek a STG system showing a normal behavior, i.e., a stress-induced transition from an R-like STG to R phase; a comparison between the abnormal system and the normal system is expected to provide the answer for the above puzzle.

From the recent STG phase diagram of Ti-Ni-Fe as shown in Fig. 9 of Ref. 19, we notice that this ternary system has a strong tendency to form R phase, as there is a large portion of R phase in the phase diagram. We then expect that this system may have a chance to transform from an R-like local order into an R phase, thus providing a chance to understand both the normal behavior of Ti-Ni-Fe STG and the abnormal behavior of Ti-Ni STG.

In the present paper, we report the existence of a normal situation: a stress-induced STG (with R-like local strain order) to martensite (R) transition in a ternary STG alloy $Ti_{50}Ni_{44.5}Fe_{5.5}$. A comparison of the different behavior of the stress-induced STG-M transition between the ternary Ti-Ni-Fe and binary Ti-Ni systems suggests that the relative thermodynamic stability of competing martensite phases determines which martensite should appear under stress. Our interpretation also well answers the question about why Ti-Ni binary STG transforms directly into $B19'$ martensite rather than passing through the R martensite.

II. EXPERIMENT

In the present study, the Ti-Ni-Fe ternary alloy with nominal composition $Ti_{50}Ni_{44.5}Fe_{5.5}$ was prepared by induction melting and casting with a mixture of 99.9% pure Ti, 99.9% pure Ni, and 99.9% pure Fe in the flow of argon gas. As Ti is a highly active metal,[20] CaO crucibles instead of graphite ones were employed in order to avoid a reaction between the container

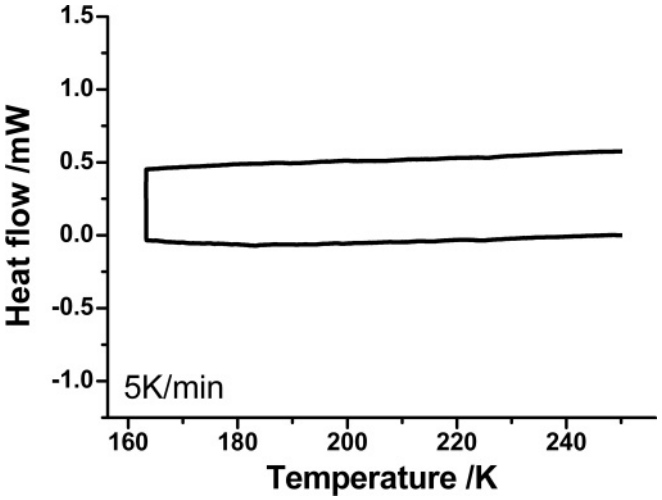

FIG. 1. DSC curve for $Ti_{50}Ni_{44.5}Fe_{5.5}$ shows no thermal peak in the whole temperature range from 163 to 250 K with the heating/cooling rate of 5 K/min.

and Ti during induction melting at high temperatures. The obtained cast ingot was spark cut and solution treated at 1000 °C for 1 h before the subsequent experiments. Quantitative chemical analysis using energy-dispersive x-ray spectroscopy (EDXS, JSM 7000F) showed that the actual composition was $Ti_{50.7}Ni_{43.7}Fe_{5.6}$.

To characterize the STG transition in the Ti-Ni-Fe samples, three sets of experiments were performed. First, a differential scanning calorimetry (DSC) test was performed with a Rigaku 822e differential scanning calorimeter to detect whether the martensitic transformation exists or not. The heating-cooling rate of DSC measurement was 5 K/min. Second, the temperature dependence of x-ray diffraction (XRD) profiles of the $Ti_{50}Ni_{44.5}Fe_{5.5}$ sample was measured to identify the possible structure change with temperature. The XRD experiment was done by using a Rigaku 2000 x-ray diffractometer equipped with a heating-cooling stage. Third, a dynamic mechanical analysis (DMA) measurement was carried out within a three-point bending mode with a TA Q800 dynamic mechanical analyzer to characterize the STG transition in our sample. The internal friction and storage modulus were recorded at four frequencies (0.1, 0.2, 0.4, and 0.8 Hz) as a function of temperature with a cooling rate of 1 K/min. In addition, TEM observation was performed at 213 and 163 K with a Hitachi H-1500 equipped with a cooling holder. The TEM specimens were mechanically polished and then punched into disks with diameters of 3 mm. Finally, the small disks were electropolished using a twin-jet apparatus operating at 260 K. The electrolytic solution consisted of 10 vol % $HClO_4$ and 90 vol % CH_3CH_2OH.

To observe the stress-induced STG-M transition in the $Ti_{50}Ni_{44.5}Fe_{5.5}$ sample, tensile testing and *in situ* XRD were performed. Tensile testing (stress-strain measurement) was performed on the same specimen as that used in the DMA measurement at four selected temperatures (185, 182, 173, and 165 K) encompassing the STG transition temperature, using a Shimadzu AG-20KNIT tensile machine. Strain gauge was used to precisely monitor the strain change during the test. Furthermore, to identify the structure change during the stress-induced STG-M transition, *in situ* XRD was carried out in the above-mentioned diffractometer with a self-made tensile stage at 185 and 165 K, respectively.

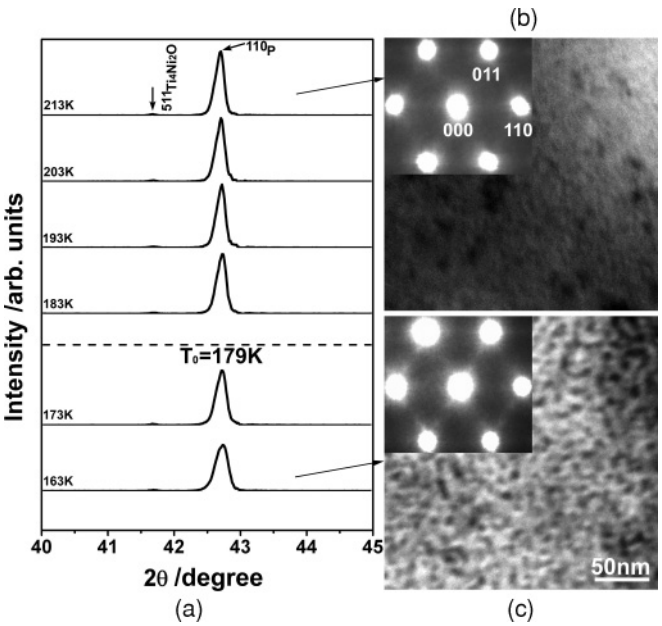

FIG. 2. (a) XRD line profiles for $Ti_{50}Ni_{44.5}Fe_{5.5}$ show that it keeps an average $B2$ structure of parent phase (P) over the entire temperature range from 213 to 163 K (the small peaks $511_{Ti_4Ni_2O}$ are used for normalization of the results). (b) and (c) show bright field images of $Ti_{50}Ni_{44.5}Fe_{5.5}$ observed at 213 and 163 K, and the insets are the corresponding diffraction patterns with $[1\bar{1}1]$ zone axis.

III. RESULTS

A. The existence of STG transition with local *R*-like strain order in $Ti_{50}Ni_{44.5}Fe_{5.5}$

As shown in the Ti-Ni-Fe ternary phase diagram,[19] the $Ti_{50}Ni_{44.5}Fe_{5.5}$ alloy is at the border between a normal R phase and STG. In the following, using a combination of DSC, XRD, DMA, and TEM observations we will show that the $Ti_{50}Ni_{44.5}Fe_{5.5}$ alloy does not undergo martensitic transition, but undergoes STG transition with local R-like strain order.

The nonexistence of long-range strain ordering or martensitic (R) transformation in this alloy is confirmed with DSC and XRD measurements in a wide temperature range. As shown in Fig. 1, the DSC result shows no signature of martensitic (R) transformation, since there is no thermal peak over a wide temperature range from 163 to 250 K. Furthermore, as shown in Fig. 2(a), the nonsplitting of a 110_{B2} XRD peak while cooling down to 163 K further confirms that the $B2$ remains down to the lowest temperature and the nonexistence of R transition. Nevertheless, a gradual broadening of the 110_{B2} peak occurs at the temperatures ranging from 213 K down to 163 K, and this will be discussed later.

In contrast to the DSC and XRD results, the DMA results of $Ti_{50}Ni_{44.5}Fe_{5.5}$ in Fig. 3 show an anomaly around 182 K, where there is a dip in the storage modulus and a peak in internal friction. This clearly demonstrates the existence of a transition. Furthermore, the dip temperature of the storage modulus and the peak temperature of internal friction show clear

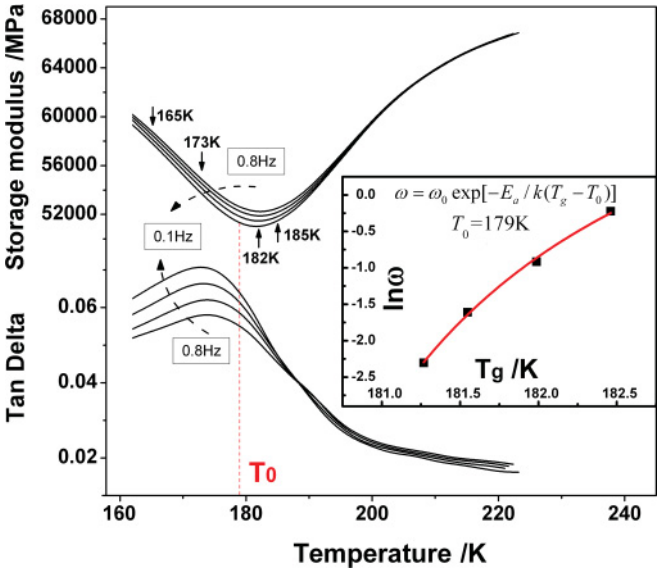

FIG. 3. (Color online) Dynamic mechanical measurement of $Ti_{50}Ni_{44.5}Fe_{5.5}$ shows an anomalous, frequency-dependent modulus dip around T_g (STG transition temperature of specific frequency) and a corresponding internal friction peak at a lower temperature. The inset shows "non-Arrhenius" T_g vs ln ω curve, fitted by the Vogel-Fulcher equation, with which T_0 is determined to be 179 K.

frequency-dependent behavior, following the Vogel-Fulcher law $\omega = \omega_0 \exp[-E_a/k(T_g - T_0)]$ (see the inset of Fig. 3) with an ideal freezing temperature $T_0 = 179$ K.[10,11] Thus Fig. 3 is critical evidence for a STG transition, being similar to other STG systems.[10,19]

The microstructure and the corresponding diffraction pattern of $Ti_{50}Ni_{44.5}Fe_{5.5}$ at 213 ($\gg T_0$) and 163 K ($\ll T_0$) are shown in Figs. 2(b) and 2(c). As shown in Fig. 2(b), although $Ti_{50}Ni_{44.5}Fe_{5.5}$ STG is unfrozen at 213 K ($\gg T_0$),[3] it is not in an ideal B2 state; it consists of "dilute" tiny nanodomains (<10 nm in size), whose diffraction pattern shows faint diffuse

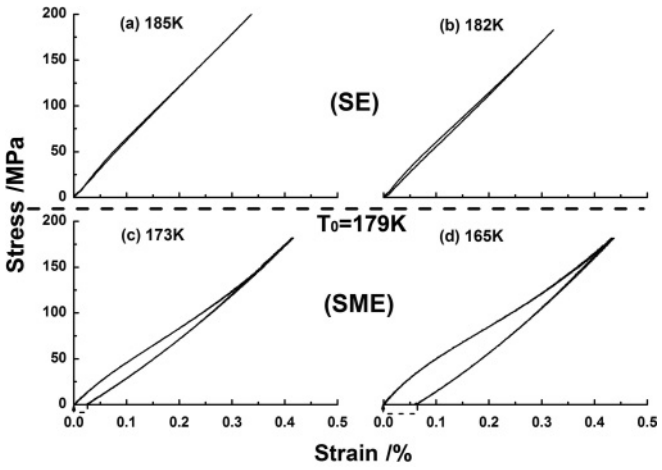

FIG. 4. Stress-strain curves for $Ti_{50}Ni_{44.5}Fe_{5.5}$ strain glass tested at four selected temperatures (shown by arrows in Fig. 3): two above T_0 [185 K in (a) and 182 K in (b)] represent superelasticity (SE), and two below T_0 [173 K in (c) and 165 K in (d)] represent shape memory effect (SME), respectively. The dashed lines in (c) and (d) denote the shape recovery process of heating above T_0.

streaks along three $\langle 110 \rangle_{B2}$ directions. In the frozen STG state ($T = 163$ K$\ll T_0$), $Ti_{50}Ni_{44.5}Fe_{5.5}$ is fully occupied by random nanodomains with a larger size (~12 nm) and the diffraction pattern shows that in addition to the diffuse streaks along $\langle 110 \rangle_{B2}$, faint diffuse spots close to the $1/3\langle 110 \rangle_{B2}$ positions [Fig. 2(c)] appear, being similar to that of a normal *R* phase. Thus it seems that the local strain order in the nanodomains is an *R*-like structure, being the same as the binary Ti-Ni STG.[10] The above TEM observation demonstrates that during a STG transition there is a gradual increase in the size and in volume fraction of the nanodomains, which have an *R*-like structure.[21,22] It is the origin of the gradual broadening of the 110_{B2} peak during cooling, as shown in Fig. 2(a).

Based on the above results, it can be concluded that the $Ti_{50}Ni_{44.5}Fe_{5.5}$ alloy does not undergo martensitic transition, but a STG transition ($T_0 = 179$ K) with local *R*-like strain order. It should be mentioned that a nominal $Ti_{50}Ni_{44.5}Fe_{5.5}$ alloy was previously reported to undergo a normal martensitic (*R*) transition,[23] being different from our observation. This is likely caused by a difference in actual composition, since this composition is close to the *R*/STG crossover composition (see the phase diagram in Ref. 19) and a small composition difference is sufficient to change a STG into a normal *R* phase.

B. Stress-induced STG to *R* martensite transition in $Ti_{50}Ni_{44.5}Fe_{5.5}$ alloy

In this section, we will present that $Ti_{50}Ni_{44.5}Fe_{5.5}$ STG shows superelasticity and shape memory effect, caused by a stress-induced transition from STG (with local *R*-like strain order) to *R* martensite.

Figure 4 shows the stress-strain curves of $Ti_{50}Ni_{44.5}Fe_{5.5}$ STG from 185 to 165 K, a temperature range encompassing $T_0 = 179$ K. At $T > T_0$ the stress-strain curves [Figs. 4(a) and 4(b)] show a superelastic behavior with a small hysteresis (which increases with lowering temperature). After an initial linear elastic behavior, the stress-strain curve shows a deviation from linearity, which is associated with a hysteresis. The deviation from linear elasticity appears around 80 MPa at 185 K [Fig. 4(a)] and about 40 MPa at 182 K [Fig. 4(b)] upon loading. At $T < T_0$ the stress-strain curves [Figs. 4(c) and 4(d)] show a plastic deformation behavior with a remnant strain after unloading, and the remnant strain increases with lowering temperature, from 0.025% to 0.063% with temperature decreasing from 173 to 165 K. Moreover, on subsequent heating the remnant strain vanishes around T_0. This is a shape memory effect. The plastic deformation of $Ti_{50}Ni_{44.5}Fe_{5.5}$ STG also shows nonlinearity upon loading. The onset stress of the nonlinearity upon loading increases from ~40 to ~50 MPa with temperature decreasing from 173 to 165 K.

It is noted that the $Ti_{50}Ni_{44.5}Fe_{5.5}$ STG does not undergo a normal *R*-phase transition down to 163 K; however, it shows superelasticity and shape memory effect. This is different from a normal martensitic alloy in which these effects originate from the martensitic transformation. Such a situation is analogous to the stress-induced STG-M transformation reported recently for a binary Ti-Ni STG.[11] However, the maximum strains for the superelasticity and shape memory effect of $Ti_{50}Ni_{44.5}Fe_{5.5}$ STG is less than 1%, much smaller than that of Ti-Ni STG. The reason for such a difference is revealed by the *in situ* XRD

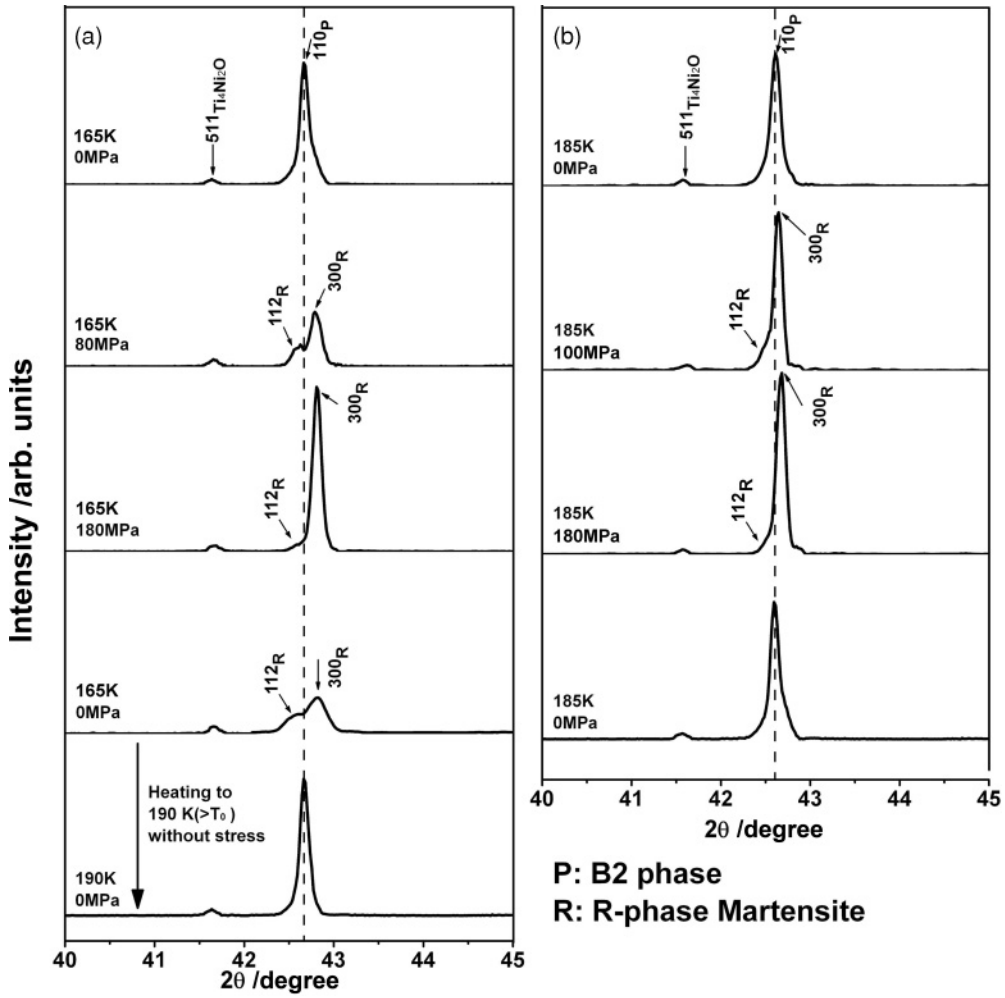

FIG. 5. *In situ* XRD evidence for the structure change during (a) a shape memory process [tensile tested at 165 K ($<T_0$) and followed by heating to 190 K ($>T_0$)] and (b) a superelasticity process [tensile loading and unloading at 185 K ($>T_0$)] for $Ti_{50}Ni_{44.5}Fe_{5.5}$ strain glass. (The straight dashed lines are drawn as a guide to the eyes.)

measurement of $Ti_{50}Ni_{44.5}Fe_{5.5}$ STG shown in Figs. 5(a) and 5(b).

Figure 5(a) shows the structure change of a STG alloy $Ti_{50}Ni_{44.5}Fe_{5.5}$ during a shape memory process, which corresponds to the stress-strain curve in Fig. 4(d). In a stress-free frozen STG state at 165 K ($<T_0$), the XRD pattern [Fig. 5(a)] showed a normal $B2$ spectrum as expected by a frozen STG. As the stress increased to about 80 MPa, the intensity of the 110_{B2} peak decreased and two new peaks appeared, which can be indexed as 112_R and 300_R, being the same as those of the normal R martensite in $Ti_{50}Ni_{48}Fe_2$ alloys.[21] When the stress reached 180 MPa [the maximum stress point in Fig. 4(a)], the 110_{B2} peak disappeared. The intensity of 300_R peaks reached maximum, while the 112_R peak remained as a small shoulder. This indicates that the 300_R planes of the stress-induced R phase are aligned mostly along the specimen surface. Since the d space of the 300_R plane is shorter than that of 110_{B2}, the cross section of the specimen shrinks by the above alignment, which corresponds to the elongation of the specimen because of the volume invariance. Subsequently, after the stress was unloaded, the 112_R peak reappeared, which corresponds to a partial strain recovery upon unloading, as shown in Fig. 4(d). When the sample was heated to 190 K ($>T_0$), the R peaks disappeared and the 110_{B2} peak reappeared; this demonstrates that the stress-induced stable R phase below T_0 transforms back to the $B2$ parent phase on heating to above T_0. This explains the shape recovery/memory of the sample. We shall further discuss the physics of the whole process in the Discussion section.

Figure 5(b) shows the structure change of the $Ti_{50}Ni_{44.5}Fe_{5.5}$ STG during a superelastic process. At 185 K (T_0+6 K), the sample showed a $B2$ diffraction pattern, as expected for an unfrozen STG.[11] When applied with a stress of 100 MPa, both the 112_R and 300_R peaks of R martensite appear and the $B2$ peak becomes smaller. This indicates that R martensite was induced from the unfrozen STG, corresponding to the stress-strain curve in Fig. 4(a). When the stress reached 180 MPa, the $B2$ reflection vanished, indicating that the unfrozen STG transformed completely into the R martensite with the alignment of 300_R planes along the surface as in the previous case. Upon stress unloading, the R martensite reflections disappeared and the $B2$ reflection reappeared, suggesting that the stress-induced R martensite is unstable above T_0, and transformed back to

the $B2$ unfrozen glassy state. Therefore, the superelasticity of STG above T_0 is attributed to a stress-induced reversible transformation from an unfrozen STG state to the R martensite.

The above *in situ* XRD result demonstrates the shape memory effect and superelasticity of $Ti_{50}Ni_{44.5}Fe_{5.5}$ STG stem from the stress-induced STG to R martensite transition, which is different from the STG to $B19'$ transition in the binary $Ti_{48.5}Ni_{51.5}$ STG. As the transformation strain of R martensite is much smaller than that of $B19'$ martensite, this explains why the maximum strain of the shape memory effect and superelasticity for $Ti_{50}Ni_{44.5}Fe_{5.5}$ STG is much smaller than that of Ti-Ni STG. It is noted that in the present ternary system, an R-like local order (the STG) transforms into an R long-range order (R phase) under stress field. This contrasts sharply with the situation observed in Ti-Ni STG, where an R-like local order (the STG) transforms into a different long-range order, $B19'$ martensite. The difference is intriguing and may indicate something important for the nature of STG. In the following section, we discuss this important issue and try to provide an answer by considering the features of the schematic free-energy landscape of STG.

IV. DISCUSSION

A. Phenomenological free-energy landscape for Ti-Ni binary and Ti-Ni-Fe ternary STGs

The schematic Landau free-energy landscape for STG, first proposed in Ref. 24, describes the state of a system in terms of both configuration coordinate and average order parameter (average strain). Such a description has two main features: (1) it enables the formation of STG and martensite and (2) it introduces the local free-energy barriers to describe the local strain-ordering effect. Such a scheme well explained many fundamental properties of STG such as the origin of STG transition and stress-induced STG-M transition. But this model has a limitation in that it assumes the instability with respect to only one kind of martensite; thus it cannot explain why the same R-like local order can result in different martensites for $Ti_{48.5}Ni_{51.5}$ and $Ti_{50}Ni_{44.5}Fe_{5.5}$ STGs.

Now we modify this schematic free-energy landscape by assuming the system has instability with respect to two different martensites: R phase and $B19'$. This assumption has gained support from known experimental observations in Ti-Ni and Ti-Ni-Fe systems, where not only $B19'$, but also R, has been observed to appear depending on different composition, temperature, and themomechanical conditions.[25,26] A typical example is the phase diagram of Ti-Ni-Fe,[19] where both R and $B19'$ exist, suggesting that these two phases are competing low-temperature phases of the system, and the system has instability with respect to both phases.

The modified schematic free-energy landscape (three dimensional) projected to free energy vs average strain plane is shown in Fig. 6, where both Ti-Ni STG and Ti-Ni-Fe STG with bi-instability are shown. For details of the description of the schematic free-energy landscape, refer to Ref. 24. Here the strain coordinate should be viewed as the strain along the transition path of the system.

Being different from the previous single instability model, the modified schematic free-energy landscape has two pairs of wells: one for R phase and the other for $B19'$. This picture is

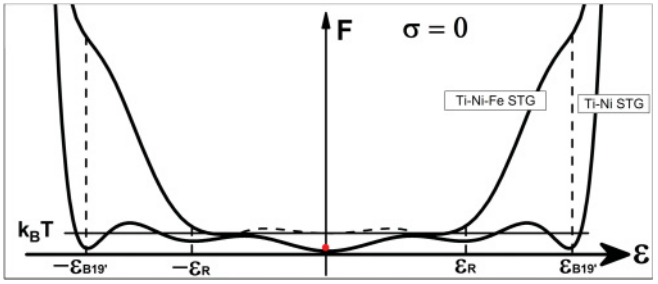

FIG. 6. (Color online) Modified schematic free-energy landscape at $\sigma = 0$ for both Ti-Ni STG and Ti-Ni-Fe STG with two martensite valleys at ε_R and $\varepsilon_{B19'}$ in a microscopic configuration-average strain (ε) space. F is the free energy; k_BT is the thermal activation energy. The valleys with average strain ε_R denote the R phase, while the valleys $\varepsilon_{B19'}$ correspond to the $B19'$ phase. The red ball denotes the current position of system in phase space. The curved solid line is for the average strain (ε) dependence of the average free energy (F) of all the microscopic configurations corresponding to a given macroscopic strain state and the difference between the upper dashed curve and the bottom solid curve represents the average energy barrier as a function of average strain (ε), which is the essential characteristic of the STG free-energy landscape.

true for both Ti-Ni and Ti-Ni-Fe alloys, but with a difference in the relative stability of the two phases, indicated by the depth of the corresponding wells. As shown in Fig. 6, Fe doping to Ti-Ni destabilizes both R and $B19'$, but has a much stronger effect to destabilize $B19'$ martensite;[25] this can also be inferred from the Ti-Ni-Fe phase diagram.[19]

B. Origin of STG transition and stress-induced STG to R-phase transition in Ti-Ni-Fe ternary alloys

Using the schematic free-energy landscape of Ti-Ni-Fe shown in Fig. 6, we now discuss the origin of STG transition in this ternary system and its stress-induced transition into R phase.

Figure 7(I) [short for Fig. 7, column (I)] shows the variation of the schematic free-energy landscape during cooling, from which we can see why the system can be frozen into a STG by carefully describing four important temperature regimes as follows:

(1) At $T > T_0 \gg T_R^*$ where T_0 is the ideal glass transition temperature and T_R^* is the instability temperature of R phase (Fig. 7 [I(a)]).

Both R and $B19'$ martensitic states are metastable and $k_BT >$ localbarrier. In such a state the system is ergodic and behaves like a normal parent phase.

(2) At $T = T_0 > T_R^*$ (Fig. 7[I(b)]).

R and $B19'$ are still metastable, but $k_BT \sim$ local barrier (caused by point defects, Fe dopant). The system begins to be trapped by local barriers and thus starts to freeze into a state with small local order parameter, an R-like local order. However, the average structure is still $B2$.

(3) At $T = T_R^* < T_0$ (Fig. 7[**I**(c)]).

$F(\varepsilon_R) = F(0)$, i.e., R reaches its instability, but $B19'$ is still metastable. As $k_BT <$ localbarrier, R - phase cannot be formed kinetically and thus the system remains a frozen STG with local R structure.

(4) At $T < T_R^* \ll T_0$ (Fig. 7[**I**(d)]).

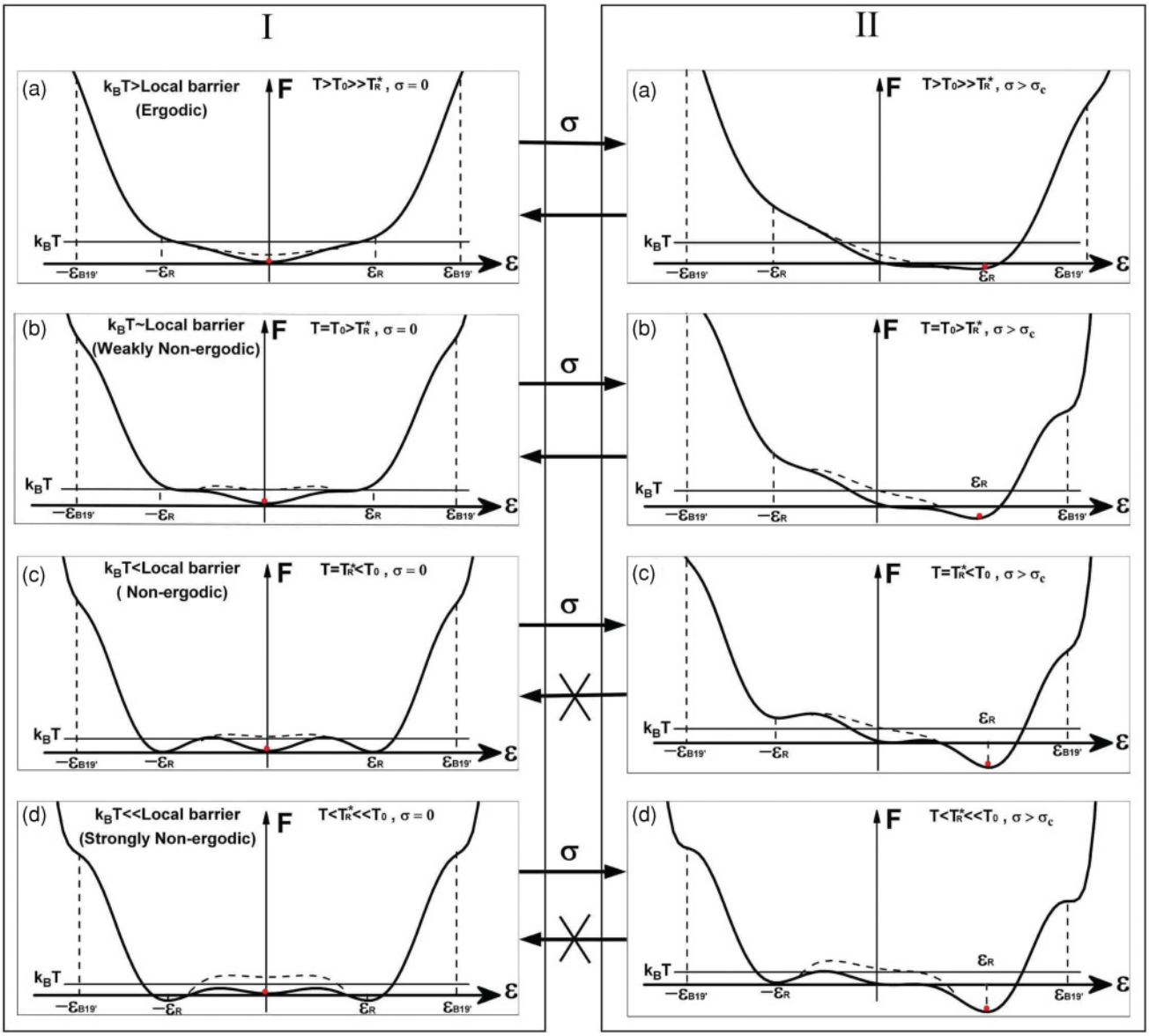

FIG. 7. (Color online) Phenomenological explanation for the STG transition and stress-induced STG-M (R phase) transition in $Ti_{50}Ni_{44.5}Fe_{5.5}$ STG. T_0 is the ideal freezing temperature at zero stress, T_R^* is the temperature where R phase starts to stabilize, and σ_C is the critical stress of the stress-induced STG-M (R phase) transition. The I column [including four curves (a), (b), (c), and (d)] shows the schematic free-energy landscape of the $Ti_{50}Ni_{44.5}Fe_{5.5}$ STG at zero stress for $T > T_0 \gg T_R^*$, $T = T_0 > T_R^*$, $T = T_R^* < T_0$, and $T < T_R^* \ll T_0$, respectively. The IIcolumn [including four curves (a), (b), (c), and (d)] shows the projected schematic free-energy landscape of strain glass at $\sigma > \sigma_C$ for $T > T_0 \gg T_R^*$, $T = T_0 > T_R^*$, $T = T_R^* < T_0$, and $T < T_R^* \ll T_0$, respectively.

The R state is thermodynamically favored, while the $B19'$ martensitic state is still metastable. As $k_BT \ll$ local barrier, R phase cannot be formed and the system still remains a frozen STG with local R structure.

Now using Figs. 7 (I) ($\sigma = 0$) and (II) ($\sigma > \sigma_C$), we provide an explanation for the superelasticity ($T \geqslant T_0$) and shape memory effect ($T < T_0$) in $Ti_{50}Ni_{44.5}Fe_{5.5}$. At $T > T_0$, the $Ti_{50}Ni_{44.5}Fe_{5.5}$ STG is in an unfrozen or ergodic state, and R phase is metastable. During stress loading, the schematic free-energy landscape is tilted as shown in Fig. 7[II(a)]. When $\sigma > \sigma_C$, the R phase becomes stable, and the system transforms into R phase but it cannot further transform into $B19'$ martensite as the latter is metastable even under stress. Upon unloading, the R phase becomes unstable again, and the system reverts to the unfrozen STG. This results in the superelasticity observed in Fig. 4(a).

At $T = T_0 > T_R^*$, i.e., the freezing temperature, the system starts to freeze. Like in the above case, loading beyond a critical stress can also transform the system into an R phase (Fig. 7[II(b)]). On the other hand, stress also lowers the freezing temperatureT_0,[24] so that the stressed system becomes unfrozen. This leads to a shape recovery upon unloading, i.e., the superelasticity.

At $T = T_R^* < T_0$, i.e., the instability temperature of the R phase, the system is frozen due to the kinetic limitation shown in Fig. 7[I(c)]. When the system is loaded with an

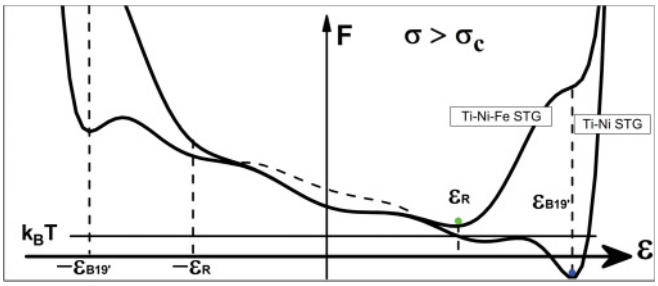

FIG. 8. (Color online) Phenomenological explanation for the phase difference of stress-induced STG-M transition in different strain glass systems: $B19'$ in $Ti_{48.5}Ni_{51.5}$ (blue ball) and R phase in $Ti_{50}Ni_{44.5}Fe_{5.5}$ (green ball) at certain temperatures. It shows the schematic free-energy landscape for both Ti-Ni STG and Ti-Ni-Fe STG at $\sigma > \sigma_C$.

external stress $\sigma > \sigma_C$, the local barriers can be overcome, and R phase now can be achieved, as shown in Fig. 7[II(c)]. As the R phase has the same thermodynamic stability as the STG at T_R^*, it remains stable after removing the external stress. Therefore, at $T = T_R^* < T_0$, the STG exhibits a plastic deformation.

At $T < T_R^* \ll T_0$, the STG is strongly frozen (Fig. 7[I(d)]). Stress loading can overcome the local barrier (but with a higher σ_C) and change the local R order into a long-range R phase (Fig. 7[II(d)]), but the induced R phase cannot recover to the original STG state because R phase is a thermodynamically stable phase at such temperature. This explains the observed plastic deformation behavior at such temperature [Figs. 4(c) and 4(d)].

For the above two plastic deformation cases (Figs. 7[II(c) and II(d)]), if the system is heated up to $T > T_0$ after unloading, the schematic free-energy landscape will change into the one in Fig. 7[I(a)], where the R state becomes unstable. Hence the system will transform back to the unfrozen STG with zero average strain and then the original shape is recovered. This explains the shape memory effect of $Ti_{50}Ni_{44.5}Fe_{5.5}$ STG below T_0, as shown in Figs. 4(c) and 4(d).

C. Phenomenological explanation for the difference in stress-induced STG-M transition between Ti-Ni STG and Ti-Ni-Fe STG

In the following, we shall explain why the product phase of stress-induced STG-M is R phase in the $Ti_{50}Ni_{44.5}Fe_{5.5}$ STG, while it is $B19'$ in $Ti_{48.5}Ni_{51.5}$, and why the formed R phase cannot be further induced into $B19'$ in $Ti_{50}Ni_{44.5}Fe_{5.5}$.

As shown in Fig. 6, there is a large difference in the relative stability of R and $B19'$ for the two systems. $B19'$ is quite unstable for $Ti_{50}Ni_{44.5}Fe_{5.5}$. Such a difference is responsible for the different transition behavior of the two systems. As shown in Fig. 8, for $Ti_{48.5}Ni_{51.5}$ STG, at $\sigma > \sigma_C$ the system directly transforms into $B19'$, because $B19'$ is more stable than R phase and the free-energy barrier between these two phases is very low. Furthermore, from Fig. 6 it can be seen that the free energy of $B19'$ martensite in $Ti_{50}Ni_{44.5}Fe_{5.5}$ STG is very high compared with the parent phase; this means that $B19'$ is very unstable. Thus in this system stress can induce the formation of R phase but cannot further induce $B19'$. Therefore, it becomes clear that the relative thermodynamic stability of the competing martensite phases (such as R phase and $B19'$) determines the product phase of stress-induced STG-M transition.

V. CONCLUSIONS

$Ti_{50}Ni_{44.5}Fe_{5.5}$ was proved to undergo a STG transition with $T_0 = 179$ K and possesses a local R-like strain order.

During the tensile testing, $Ti_{50}Ni_{44.5}Fe_{5.5}$ STG exhibited shape memory effect below T_0 and superelasticity above T_0. These effects originate from a new stress-induced STG (local R-like strain order) to R-phase transition, which is different from that found in $Ti_{48.5}Ni_{51.5}$ (local R-like STG $\rightarrow B19'$). Our findings suggest that the stress-induced STG-M transition may be a general phenomenon for many STG systems.

A modified phenomenological model has been proposed and used to explain the origin of STG transition and stress-induced STG-M transition in Ti-Ni-based STG. The competition of thermodynamic stabilities between different martensite phases is responsible for different product phases of the stress-induced STG-M transition, which may shed light on the understanding of field-induced long-range transition in other ferroic glass systems, such as relaxor ferroelectrics.

ACKNOWLEDGMENTS

The present work was supported by Grant-in-Aid for Scientific Research (B) of JSPS, National Science Foundation of China (Grants No. 50720145101 and No. 50771079), and National Basic Research Program of China under Grant No. 2010CB631003 as well as NCET and 111 Project of China (B06025). J.Z. acknowledges funding by the research center of SFB 459 ("Shape Memory Technology") at the Ruhr-University Bochum, and also the funding by Alexander von Humboldt Foundation. The authors thank T. Suzuki, D. Wang, and G. L. Fan for technical support and helpful discussions.

*Author to whom correspondence should be addressed. Ren.Xiaobing@nims.go.jp

[1] J. A. Mydosh, *Spin Glasses* (Taylor & Francis, Philadelphia, 1993).
[2] J. Hessinger and K. Knorr, Phys. Rev. Lett. **65**, 2674 (1990); Phys. Rev. B **47**, 14813 (1993).
[3] Y. Wang, X. Ren, K. Otsuka, and A. Saxena, Phys. Rev. B **76**, 132201 (2007).
[4] Z. Kutnjak, C. Filipič, R. Pirc, A. Levstik, R. Farhi, and M. El Marssi, Phys. Rev. B **59**, 294 (1999).
[5] B. Jerome and J. Commandeur, Nature (London) **386**, 589 (1997).

[6]K. Binder and A. P. Young, Rev. Mod. Phys. **58**, 801 (1986).
[7]L. Santen and W. Krauth, Nature (London) **405**, 550 (2000).
[8]C. A. Angell, Science **267**, 1924 (1995).
[9]S. R. Shenoy and T. Lookman, Phys. Rev. B **78**, 17 (2008).
[10]S. Sarkar, X. Ren, and K. Otsuka, Phys. Rev. Lett. **95**, 205702 (2005).
[11]Y. Wang, X. B. Ren, and K. Otsuka, Phys. Rev. Lett. **97**, 225703 (2006).
[12]S. Semenovskaya and A. G. Khachaturyan, Acta Mater. **45**, 4367 (1997).
[13]A. G. Khachaturyan, *Theory of Structural Transformation in Solids* (Wiley Interscience, New York, 1983).
[14]P. Lloveras, T. Castan, M. Porta, A. Planes, and A. Saxena, Phys. Rev. Lett. **100**, 165707 (2008).
[15]P. Lloveras, T. Castan, M. Porta, A. Planes, and A. Saxena, Phys. Rev. B **80**, 054107 (2009).
[16]E. V. Colla, N. K. Yushin, and D. Viehland, J. Appl. Phys. **83**, 3298 (1998).
[17]J. L. Dellis, M. El Marssi, P. Tilloloy, R. Farhi, and D. Viehland, Ferroelectrics **201**, 167 (1997).
[18]A. A. Bokov and Z. G. Ye, J. Mater. Sci. **41**, 31 (2006).
[19]D. Wang, Z. Zhang, J. Zhang, Y. Zhou, Y. Wang, X. Ding, Y. Wang, and X. Ren, Acta Mater. **58**, 6206 (2010).
[20]J. Zhang, G. L. Fan, Y. M. Zhou, X. D. Ding, K. Otsuka, K. Nakamura, J. Sun, and X. B. Ren, Acta Mater. **55**, 2897 (2007).
[21]M. S. Choi, T. Fukuda, T. Kakeshita, and H. Mori, Philos. Mag. **86**, 67 (2006).
[22]Y. Murakami and D. Shindo, Philos. Mag. Lett. **81**, 631 (2001).
[23]M. S. Choi *et al.*, Philos. Mag. **88**, 2449 (2008).
[24]Y. Wang, X. Ren, K. Otsuka, and A. Saxena, Acta Mater. **56**, 2885 (2008).
[25]X. Ren *et al.*, Mater. Sci. Eng., A **312**, 196 (2001).
[26]K. Otsuka and X. Ren, Prog. Mater Sci. **50**, 511 (2005).